Bose-Einstein Condensation in a Tightly Confining dc Magnetic Trap

M.-O. Mewes, M. R. Andrews, N. J. van Druten, D. M. Kurn, D. S. Durfee, and W. Ketterle

Department of Physics and Research Laboratory of Electronics, Massachusetts Institute of Technology, Cambridge, Massachusetts 02139

(Received 17 May 1996)

Bose-Einstein condensation of sodium atoms has been observed in a novel "cloverleaf" trap. This trap combines tight confinement with excellent optical access, using only dc electromagnets. Evaporative cooling in this trap produced condensates of 5×10^6 atoms, a tenfold improvement over previous results. We measured the condensate fraction and the repulsive mean-field energy, finding agreement with theoretical predictions. [S0031-9007(96)00729-6]

PACS numbers: 03.75.Fi, 05.30.Jp, 32.80.Pj, 64.60.–i

Einstein predicted in 1925 that an ideal quantum gas would undergo a phase transition when the thermal de Broglie wavelength becomes larger than the mean spacing between particles [1]. For many years, this phenomenon, now known as Bose-Einstein condensation (BEC), was regarded as a mathematical artifact, until London "rediscovered" it in 1938 to explain the superfluidity of liquid helium [2]. However, in liquid helium, the purely quantum-statistical nature of the BEC transition is complicated by strong interactions [3]. BEC was recently created in excitons, which behave similarly to a gas of particles [4]. Bose-Einstein condensation in dilute atomic gases was first pursued in spin-polarized hydrogen [5], and last year was finally observed in alkali vapors at JILA and MIT [6,7]. A third group, at Rice University, reported cooling of lithium atoms into the quantum-degenerate regime [8]. These experiments led to renewed experimental and theoretical interest in the study of quantum-degenerate gases [9].

In this Letter, we report a detailed study of the properties of a weakly interacting condensate and a comparison with theory [10]. These experiments were carried out in a novel atom trap which overcame major limitations of the traps used so far for evaporative cooling and BEC: the time-dependent field in the case of the TOP trap [11], the sensitivity to shape and position of the optical plug in the optically plugged trap [7], the inflexibility of a trap that uses permanent magnets [8], or the constraints of a cryogenic environment for a trap that employs superconducting coils [5].

Our new trap is of the Ioffe-Pritchard (IP) type, suggested in Refs. [12,13] and originally used for trapping hydrogen [14,15] and sodium [16] in cryogenic traps. In contrast, our trap is built with normal electromagnets. Previously, it had been concluded that IP traps are inferior in confinement compared to the TOP trap [11], which uses a static spherical quadrupole field and a rotating bias field. However, the previous analysis was incomplete, and we point out here that spin flips induced by the rotating field limit the confinement of a TOP trap to below the value that can be achieved in an IP trap. Tight confinement is crucial because evaporative cooling [17] (the technique used to attain BEC in atomic gases) requires densities high enough that the thermalization time is much shorter than the lifetime of the sample.

The design of our trap was based on the following considerations. The magnetic trapping potential μB is given by the effective magnetic moment μ of the atom and the absolute value B of the magnetic field. Both the TOP and IP traps are harmonic and cylindrically symmetric near the minimum of the potential, with different radial and axial curvatures. The geometric mean of the curvatures is the relevant figure of merit of a trap for evaporative cooling [18]. The radial curvature B''_{IP} in an IP trap varies with the radial gradient B' and the bias field B_0 as $B''_{\mathrm{IP}} \approx B'^2/B_0$. In the TOP trap, one obtains for the curvature $B''_{\mathrm{TOP}} = B'^2/2B_{\mathrm{rot}}$, where B_{rot} is the amplitude of the rotating bias field. Stability against spin flips requires the Larmor frequency (which is proportional to B_0 or B_{rot}) to be much higher than ω_{rot}, the frequency at which the moving atom sees the inhomogeneous magnetic field rotate. For an IP trap, ω_{rot} is less than or equal to the atomic oscillation frequency, whereas in a TOP trap, the frequency of the rotating field ω_{rot} must be much higher than the atomic oscillation frequency (in Ref. [6], for example, the ratio of ω_{rot} to the radial trap frequency was 150). As a consequence, the minimum B_{rot} of a TOP trap must be much larger than B_0 of an IP trap. This limits the radial curvature of the TOP trap to be about 2 orders of magnitude weaker than that of an IP trap with comparable radial gradient B'. In the axial direction, the TOP trap creates a B'' which can be a hundred times larger than in an IP trap; however, the product of the three curvatures is higher for an optimized IP trap. The above discussion assumes that the curvature does not change over the extent of the cloud and is thus valid for cold samples.

A somewhat different discussion applies when a warmer cloud of temperature T is loaded into a magnetic trap. In the TOP trap, B_{rot} must be larger than $20kT/\mu$ to maintain a trap depth larger than $5kT$, determined by the rotating zero of the magnetic field. The resulting

 0031-9007/96/77(3)/416(4)$10.00

radial curvature of $\mu B'^2/40kT$ is much lower than the effective curvature $\mu B'^2/kT$ of the IP trap [17]. Again, the IP trap has a higher mean curvature.

The usual configuration of the IP trap, using the so-called "Ioffe bars" or the baseball winding pattern [19], limits optical access to the trapping region. This was solved by a novel winding pattern, allowing full 2π optical access in the symmetry plane of the trap: each of the two axial coils (the so-called "pinch coils" [19]) was surrounded by four coils, in the form of planar cloverleaves, which created the radial quadrupole field. Two larger axial coils were added to reduce the bias field. The twelve coils of the "cloverleaf" trap allowed independent and almost orthogonal control over the three important parameters of the trapping field: axial bias field, axial curvature, and radial gradient. Additional coils generated bias fields along the x, y, and z directions, allowing accurate overlap of the centers of the light trap and the magnetic trap.

The experimental procedure was as follows. A high density of magnetically trapped sodium atoms was obtained in a multistep procedure similar to that described in our previous works [7,20]. Using a Zeeman slower and a dark SPOT [21], within 2 s typically $(5-10) \times 10^9$ atoms were confined at densities of 5×10^{11} cm^{-3}. *In situ* loading of the magnetic trap was accomplished by extinguishing the laser-cooling light quickly and switching on the cloverleaf trap with the maximum values of axial curvature ($\approx$125 G/cm^2), radial gradient ($\approx$170 G/cm), and axial bias field ($\approx$100 G) within 1 ms. The trapping potential was approximately isotropic and provided confinement at about the same temperature and size as the initial laser-cooled cloud. This resulted in typically 2×10^9 trapped atoms in the $F = 1, m_F = -1$ state, at a peak density of 6×10^{10} cm^{-3} and a phase space density $\approx 10^6$ times lower than required for BEC. The elastic collision rate in the center of the cloud was about 20 Hz, based upon an elastic collision cross section of 6×10^{-12} cm^2 [20]. Subsequently, the cloud was radially compressed by reducing the bias field to 1 G. The lifetime of the trapped atoms was approximately 1 min, probably limited by background-gas scattering at a pressure of typically 3×10^{-11} mbar. From Hall-probe measurements of the magnetic fields, the axial and radial trapping frequencies were calculated to be $\omega_x = 2\pi \times 18$ Hz and $\omega_y = \omega_z = 2\pi \times 320$ Hz, respectively.

The atoms were further cooled by rf-induced evaporation [11,17,20,22]. The rf frequency was swept from 30 MHz to a variable final value, typically around 1 MHz. The sweep time (between 15 and 26 s) was longer than in our previous experiment [7], where such a long evaporation time did not result in more efficient cooling. This suggests that some additional heating process was present in our previous trap.

After evaporation, the atom cloud was allowed to thermalize in the magnetic trap for 100 ms, with the rf switched off. Finally, following a sudden switch-off of the trap and a variable delay time, the atom cloud was imaged using the same method as in our previous work [7]. The probe laser beam was directed vertically through the atom cloud, along a radial axis of the trap, and the probe absorption was imaged onto a charge-coupled device sensor with a system of lenses having a resolution of 5 μm. The vertical absorption beam allowed for delay times of up to 50 ms (corresponding to a drop distance of 1.2 cm). No refocusing was necessary due to the expansion of the falling cloud. Density, temperature, and total number of atoms were determined from these absorption images, as will be described below.

As in our previous work [7], the BEC phase transition was observed as the sudden appearance of a bimodal distribution in time-of-flight images when the final rf frequency was lowered below a critical value of typically 1.1 MHz. Examples of time-of-flight images are shown in Fig. 1, for varying delay times; they show the expansion of the initially pencil-shaped cloud. The normal component expands isotropically, whereas the condensate expands predominantly along the radial direction.

For the longer flight times, the image reflects the velocity distribution of the expanding thermal cloud because the initial spatial extent is negligible. We analyzed such images taken with a 40 ms time of flight, and a varying final rf frequency. At the transition temperature and below, the velocity distribution of the normal component is isotropic and proportional to $g_{3/2}[\exp(-mv^2/2kT)]$ where $g_{3/2}$ is the familiar Bose function. On the other hand, in the Thomas-Fermi regime (see below) the density distribution of the expanding condensate is anisotropic

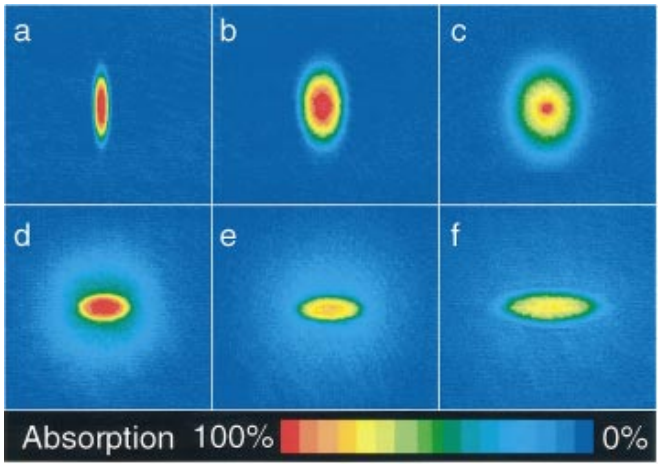

FIG. 1(color). Time-of-flight images of expanding mixed clouds. Flight times for (a)–(f) are 1, 5, 10, 20, 30, and 45 ms, respectively. The normal component expands isotropically [most clearly seen in (d) and (e), the light-blue spherical cloud], whereas the condensate expands much faster in the radial than in the axial direction. The earliest image shows the pencil-like shape of the initial cloud. In the early phase of the expansion, the clouds appear larger than their true sizes due to complete absorption of the probe laser light. The width of the field of view is 1.6 mm.

and predicted to maintain its parabolic shape [23]. Full two-dimensional images were fitted assuming this model for the expansion of the cloud. The shape of the condensate was clearly non-Gaussian and was fitted well by the parabolic function. The relatively low optical density of the normal fraction limited the determination of an accurate temperature to clouds with condensate fractions smaller than 50%.

Theoretically, one expects a critical temperature T_c of [24]

$$kT_c = \hbar\bar{\omega}(N/1.202)^{1/3}, \quad (1)$$

with N the number of atoms and $\bar{\omega}$ the geometric mean of the harmonic trap frequencies $\bar{\omega} = (\omega_x\omega_y\omega_z)^{1/3}$. Below the critical temperature, the condensate fraction should vary as [24]

$$N_0/N = 1 - (T/T_c)^3. \quad (2)$$

In Fig. 2, the condensate fraction is plotted versus normalized temperature $T/N^{1/3}$ (both determined from the fits) and compared to the theoretical prediction, Eq. (2). As the temperature was lowered by evaporative cooling, the number of atoms N decreased. The data were plotted in terms of $T/N^{1/3}$ to account for the scaling of T_c with N, Eq. (1). The scatter in the experimental data is consistent with our estimated statistical and systematic errors. Comparing the horizontal scales of the theoretical and experimental data yields [using Eq. (1)] $\bar{\omega} = 2\pi \times 142$ Hz, in reasonable agreement with $\bar{\omega} = 2\pi \times 120$ Hz, as determined from the Hall-probe measurements.

Note that Eqs. (1) and (2) are equivalent to $N - N_0 = 1.202(kT/\hbar\bar{\omega})^3$, expressing that the normal component behaves as a saturated vapor where the interaction energy is much smaller than the thermal energy. Therefore, the condensate fraction is only weakly affected by interactions between the atoms.

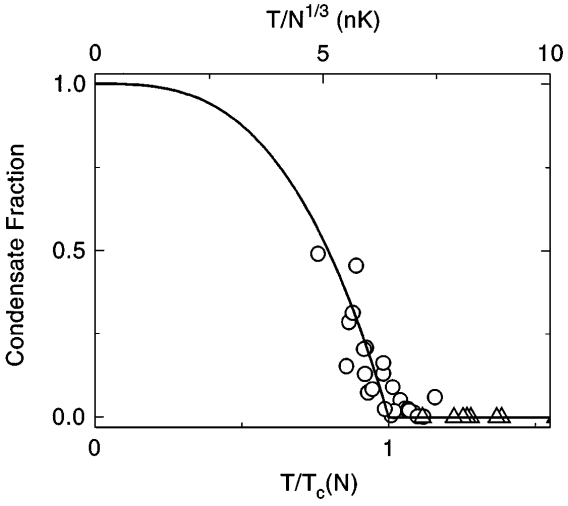

FIG. 2. Condensate fraction versus normalized temperature $T/T_c \propto T/N^{1/3}$. Solid line: theoretical curve, Eq. (2). The experimental data were determined from fits to time-of-flight images (see text); △: clouds with no detectable condensate, ○: clouds with both condensate and normal fraction visible.

Typical values for the number of atoms and temperature at the phase transition were $N_c = 15 \times 10^6$ and $T_c = 2\ \mu$K, respectively. The critical peak density at $2\ \mu$K was 1.5×10^{14} cm^{-3}. Pure condensates with up to 5×10^6 atoms have been observed, a factor of 10 improvement over our previous result [7], which is ascribed to the more efficient evaporative cooling in the cloverleaf trap.

If the density of condensed atoms is high, the kinetic energy of the condensate is negligible compared to its interaction energy $n_0\tilde{U}$ (Thomas-Fermi approximation), where n_0 is the peak condensate density, and $\tilde{U}$ is proportional to the scattering length a [25]: $\tilde{U} = 4\pi\hbar^2 a/m$ ($\tilde{U}/k = 1.3 \times 10^{-21}$ K cm^3). In this regime, the condensate density distribution is given by $n_0(\mathbf{r}) = n_0 - V(\mathbf{r})/\tilde{U}$, where $V(\mathbf{r})$ is the trapping potential [and $n_0(\mathbf{r})$ vanishes where $V(\mathbf{r}) > n_0\tilde{U}$]. This results in a peak condensate density

$$n_0 = 0.118(N_0 m^3\bar{\omega}^3/\hbar^3 a^{3/2})^{2/5}. \quad (3)$$

For typical parameters of our experiment, $n_0 = 3.0 \times 10^{14}$ cm^{-3}, and the mean-field energy per atom, $2n_0\tilde{U}/7$, is 110 nK, much larger than the zero-point energy of 16 nK. Consequently, the assumption of negligible kinetic energy is justified.

In the Thomas-Fermi approximation, the aspect ratio of the condensate is the ratio of radial and axial trapping frequencies, which is approximately 20. The initial acceleration after switch-off of the trap is determined by the gradient of the interaction energy and is inversely proportional to the width of the condensate. Consequently, the aspect ratio of the velocity distribution is inverted compared to the initial spatial distribution. In our case, nearly all the interaction energy is released in the radial expansion. The axial expansion corresponds to a temperature around 0.2 nK, and is small compared to the initial length. The radial kinetic energy obtained from the time-of-flight images corresponds therefore to the interaction energy of the condensate.

In Fig. 3, the interaction energy is plotted versus the number of atoms in the condensate. N_0 was varied by only partially condensing the cloud, or by using rf evaporation to remove atoms from a pure condensate. As can be seen from the figure, the expansion of the condensate did not depend on whether a normal component was present. This indicates that interactions with the normal fraction did not affect the expansion of the condensate. The mean-field energy per condensed atom is proportional to $N_0^{2/5}$, as predicted by Eq. (3). From the proportionality constant a value for the scattering length was obtained.

To eliminate errors due to uncertainty in the trapping frequencies and absolute measurements of atom numbers, $\bar{\omega}^3$ in Eq. (3) was expressed by using Eqs. (1) and (2). In this way we find $a = 65 \pm 30$ bohr, which agrees well with $a = 92 \pm 25$ bohr, the value previously determined from thermal relaxation times [20]. The determination of the released energy per atom, $2n_0\tilde{U}/7$, provides a direct

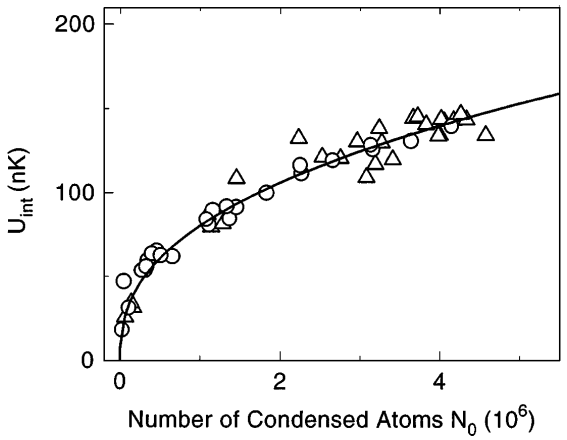

FIG. 3. Mean-field energy per condensed atom versus the number of atoms in the condensate. △: clouds with no visible normal fraction. ○: clouds with both normal and condensed fractions visible. The solid line is a fit proportional to $N_0^{2/5}$.

measurement of the peak density n_0 of the condensate, and, combined with N_0, of the size of the condensate. For $N_0 = 5 \times 10^6$, the Thomas-Fermi approximation gives a density distribution of the condensate which is nonzero within 17 μm in the radial direction and 300 μm axially [25]. Note that these widths are much larger than the rms widths of the ground state, $\sqrt{2\hbar/m\omega}$, which are 1.7 μm in the radial and 7.0 μm in the axial directions.

The condensate had a lifetime of about 20 s when the rf radiation was left on. This lifetime decreased to about 1 s when the rf field was turned off. This reduced lifetime might be caused by grazing-incidence collisions with 300 K background-gas atoms, which excite trapped atoms to an energy comparable to the trap depth of about 5 mK. If these hot atoms are kept in the trap, they rapidly heat up the condensate. If the rf is left on, it skims off such atoms. A more detailed study is needed to accurately characterize the decay of the condensate.

In conclusion, we have achieved Bose-Einstein condensation of sodium atoms in a novel cloverleaf trap, a purely magnetic trap using only dc electromagnets. The variable confinement and aspect ratio of the cloverleaf trap are ideal for studying various properties of the condensate. In the present case the condensate had an aspect ratio of $\approx$20 and a maximum length of 300 μm. The kinetic energy of the axial motion is about 1 pK. An elongated condensate is advantageous for several experiments. For instance, it is possible to spatially resolve the shape of the condensate amidst the normal fraction [26]. Also, an elongated condensate can easily be cut with a sheet of far-off-resonant blue-detuned light [7]. This configuration might realize an atomic Josephson junction, or can be used to perform interference experiments with two condensates, demonstrating the existence of a macroscopic wave function and superfluidity.

We are grateful to Dan Kleppner for helpful comments on the manuscript. This work was supported by ONR, NSF, JSEP, and the Sloan Foundation. M.-O. M. and D. M. K. acknowledge support from Studienstiftung des Deutschen Volkes and an NSF Graduate Research Fellowship, respectively, and N. J. v. D. from "Nederlandse Organisatie voor Wetenschappelijk Onderzoek (NWO)" and NACEE (Fulbright fellowship).

[1] A. Einstein, Sitz. K. Preuss. Akad. Wiss. **1925**, 3 (1925).
[2] F. London, Nature (London) **141**, 643 (1938).
[3] *Bose-Einstein Condensation*, edited by A. Griffin, D. W. Snoke, and S. Stringari (Cambridge University Press, Cambridge, UK, 1995).
[4] Jia Ling Lin and J. P. Wolfe, Phys. Rev. Lett. **71**, 1222 (1993).
[5] T. J. Greytak, in Ref. [3], pp. 131–159.
[6] M. H. Anderson *et al.*, Science **269**, 198 (1995).
[7] K. B. Davis *et al.*, Phys. Rev. Lett. **75**, 3969 (1995).
[8] C. C. Bradley, C. A. Sackett, J. J. Tollett, and R. G. Hulet, Phys. Rev. Lett. **75**, 1687 (1995).
[9] Book of Abstracts, Workshop on Collective Effects in Ultracold Atomic Gases, Les Houches, France, 1996 (to be published).
[10] Related results were obtained at JILA (to be published).
[11] W. Petrich, M. H. Anderson, J. R. Ensher, and E. A. Cornell, Phys. Rev. Lett. **74**, 3352 (1995).
[12] Y. V. Gott, M. S. Ioffe, and V. G. Telkovsky, in *Nuclear Fusion, 1962 Suppl., Pt. 3* (International Atomic Energy Agency, Vienna, 1962), pp. 1045–1049, 1284.
[13] D. E. Pritchard, Phys. Rev. Lett. **51**, 1336 (1983).
[14] H. F. Hess *et al.*, Phys. Rev. Lett. **59**, 672 (1987).
[15] R. van Roijen, J. J. Berkhout, S. Jaakkola, and J. T. M. Walraven, Phys. Rev. Lett. **61**, 931 (1988).
[16] V. S. Bagnato *et al.*, Phys. Rev. Lett. **58**, 2194 (1987).
[17] W. Ketterle and N. J. van Druten, in Advances in Atomic, Molecular and Optical Physics, edited by B. Bederson and H. Walther (Academic Press, San Diego, to be published), Vol. 37.
[18] The BEC transition temperature and the collision rate after adiabatic compression are proportional to this quantity which therefore determines the efficiency of evaporative cooling [17].
[19] T. Bergeman, G. Erez, and H. J. Metcalf, Phys. Rev. A **35**, 1535 (1987).
[20] K. B. Davis *et al.*, Phys. Rev. Lett. **74**, 5202 (1995).
[21] W. Ketterle *et al.*, Phys. Rev. Lett. **70**, 2253 (1993).
[22] Originally suggested by D. E. Pritchard, K. Helmerson, and A. G. Martin, in *Atomic Physics 11*, edited by S. Haroche, J. C. Gay, and G. Grynberg (World Scientific, Singapore, 1989), pp. 179–197, and first realized by W. Ketterle *et al.*, in Proceedings of the OSA Annual Meeting, Toronto, Canada, 1993 (unpublished).
[23] R. Dum and Y. Castin (to be published).
[24] S. R. de Groot, G. J. Hooyman, and C. A. ten Seldam, Proc. R. Soc. London A **203**, 266 (1950).
[25] G. Baym and C. J. Pethick, Phys. Rev. Lett. **76**, 6 (1996), and references therein.
[26] M. R. Andrews *et al.*, Science (to be published).